ACS Catalysis

Research Article

pubs.acs.org/acscatalysis

NO Chemisorption on Cu/SSZ-13: A Comparative Study from Infrared Spectroscopy and DFT Calculations

Renqin Zhang,[†] Jean-Sabin McEwen,*[,†,‡,§] Márton Kollár,[∥] Feng Gao,[∥] Yilin Wang,[∥] János Szanyi,[∥] and Charles H.F. Peden*[,∥]

[†]The Gene and Linda Voiland School of Chemical Engineering and Bioengineering, Washington State University, Pullman, Washington 99164, United States

[‡]Department of Physics and Astronomy, Washington State University, Pullman, Washington 99164, United States

[§]Department of Chemistry, Washington State University, Pullman, Washington 99164, United States

[∥]Institute for Integrated Catalysis, Pacific Northwest National Laboratory, Richland, Washington 99352, United States

Supporting Information

ABSTRACT: The locations and energies of Cu ions in a Cu/SSZ-13 zeolite catalyst were investigated by density functional theory (DFT) calculations. For "naked" Cu^{2+} ions (i.e., Cu^{2+} ions with no ligands in their coordination spheres other than zeolite lattice oxygen atoms), the more energetically favorable sites are within a 6-membered ring. However, with the presence of various adsorbates, the energy difference between 6- and 8-membered ring locations greatly diminishes. Specifically, Cu^{2+} ions are substantially stabilized by −OH ligands (as $[Cu^{II}(OH)]^+$), making the extra-framework sites in an 8-membered ring energetically more favorable than 6-membered ring sites. Under fully dehydrated high vacuum conditions with different Si/Al and Cu/Al ratios, three chemisorbed NO species coexist upon exposure of NO to Cu/SSZ-13: NO^+, Cu^{2+}−NO, and Cu^+−NO. The relative signal intensities for these bands vary greatly with Si/Al ratios. The vibrational frequency of chemisorbed NO was found to be very sensitive to the location of Cu^{2+} ions. On the one hand, with the aid from DFT calculations, the nature for these vibrations can be assigned in detail. On the other hand, the relative intensities for various Cu^{2+}−NO species provide a good measure of the nature of Cu^{2+} ions as functions of Si/Al and Cu/Al ratios and the presence of humidity. These new findings cast doubt on the generally accepted proposal that only Cu^{2+} ions located in 6-membered rings are catalytically active for NH_3−SCR.

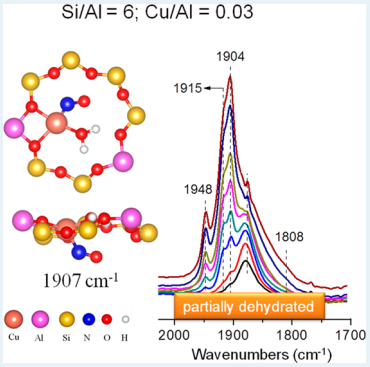

KEYWORDS: *infrared spectroscopy, DFT, NO chemisorption, oxidation state, Cu/SSZ-13, dehydration, Brønsted acid site*

1. INTRODUCTION

In the past few years, small-pore copper-ion-exchanged zeolite catalysts (Cu/SSZ-13) with a chabazite (CHA) structure have been commercialized as part of the emission control systems for diesel passenger vehicles and light-, medium-, and heavy-duty trucks in the U.S. and Europe, due to their remarkable activity and hydrothermal stability for the NH_3 selective catalytic reduction (SCR) process.[1−4] Along with studies aimed at assessing the properties of the Cu/SSZ-13 catalysts under practical engine exhaust operating conditions, considerable recent research has also focused on the fundamental chemical and physical properties of this interesting catalytic material.

Initial reports suggested that Cu ions are located only in the 6-membered rings of the primary double 6-membered ring structures of this CHA zeolite.[5−7] However, recent studies have revealed that Cu ions can occupy more than one ion-exchange site. The results of H_2 temperature-programmed reduction, zeolite framework T−O−T vibrations, and electron paramagnetic resonance (EPR) experiments during dehydration also suggested facile movement of copper ions in the presence of strongly interacting adsorbates (e.g., H_2O).[8−10] A recent in operando X-ray absorption spectroscopy (XAS) studied by Riberio and co-workers has concluded that the "standard" (i.e., NO_x = NO) NH_3 SCR reaction proceeds via a redox mechanism between Cu^{2+} and Cu^+ oxidation states.[11,12] This conclusion was drawn because under "fast" and "NO_2" SCR conditions, in which NO_2 is half or all of the NO_x feed, respectively, Cu^{2+} remains as the only evident Cu oxidation state. Under the more reducing "standard" SCR conditions, where there is no NO_2 in the feed, a Cu^+ species is evident in the XAS data.[12] In line with such a redox mechanism, Cu^{2+} can, in principle, be reduced to Cu^+ by either NH_3 or NO, and Cu^+ can then be oxidized by O_2 to Cu^{2+} to finish the redox cycling. In our recent FTIR and NMR spectroscopic study of NO and Cu/SSZ-13 interactions, we suggested that Cu^{2+} can be reduced to Cu^+ by NO, leading to the formation of the spectroscopically observed Cu−nitrosyl complex (Cu^+−NO^+).[3,13,14] Based on the spectroscopic evidence, a "standard"

Received: April 25, 2014
Revised: September 9, 2014
Published: September 26, 2014

   dx.doi.org/10.1021/cs500563s | ACS Catal. 2014, 4, 4093−4105

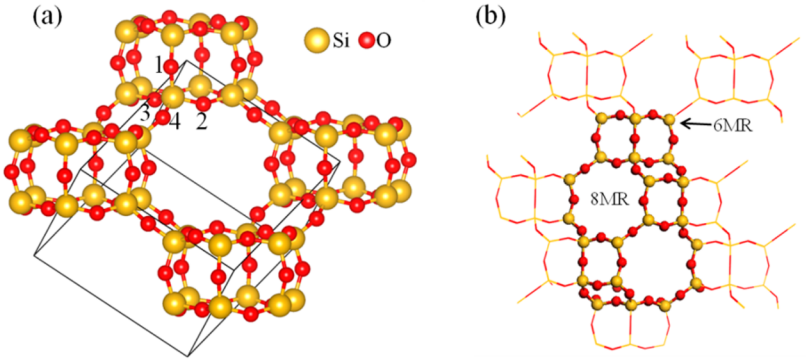

Figure 1. (a) Structure of a pure SSZ-13 zeolite belonging to the chabazite zeolite family, in which the rhombohedral unit cell used in our calculations is shown. The rhombohedral unit cell contains 12 Si and 24 O atoms. There are four nonequivalent O sites, which are labeled by numbers 1−4; their differences are described in the main text. (b) Another view of the chabazite structure (see ref 4). Large yellow and small red balls represent Si and O atoms, respectively.

SCR mechanism that involves such a Cu−nitrosyl complex has been proposed.[3,13]

The first application of density functional theory (DFT) methods to the modeling of NO_x catalysis on Cu zeolites was done with single- and multi-T-site cluster models.[15−18] These computational results are helpful for understanding the catalytic activity and reaction mechanism(s) on Cu-exchanged zeolites. For example, for the decomposition of NO on Cu-exchanged zeolites,[16] it was found that there is evidence for a pathway involving two successive O atom transfers to an isolated, zeolite-bound Cu^+ center, initiated by the formation of a short-lived and difficult to detect isonitrosyl intermediate, and yielding sequentially N_2O and Cu-bound O followed by N_2 and Cu-bound O_2. Such models have been shown to be generally in good agreement with fully periodic models, although interactions, in particular with H_2O, and more extended portions of the lattice are only fully captured with periodic models.[12] Such periodic models have been actively used to study the SSZ-13 zeolite.[4,12,19−25] Göltl et al. predicted a distribution of active sites at different levels of ion exchange by considering the energetic variations of the Cu locations in Cu/SSZ-13.[24] Although an isolated Cu^{2+} ion in Cu/SSZ-13 has been suggested to be an active site under SCR conditions,[7] further studies suggested that the nature of the Cu species in Cu/SSZ-13 is dependent on the Si/Al and Cu/Al atomic ratios.[22,23] With the aid of periodic DFT calculations, it was found that for a series of Si/Al = 4.5 samples with various Cu loadings, the dominant Cu ion configuration is an isolated Cu^{2+} ion in Cu/SSZ-13 with a Cu/Al atomic ratio below 0.2, while Cu_xO_y species in the 8-membered ring of Cu/SSZ-13 also form when the Cu/Al ratio is above 0.2.[23] However, only the isolated Cu^{2+} ions were claimed to be the SCR active centers while Cu_xO_y species were suggested to be inert. This conclusion is somewhat surprising because prior studies on other Cu/zeolite SCR catalysts (Cu/ZSM-5, Cu/beta, Cu/Y, etc.) seem to agree in general that a Cu-ion dimer species is a particularly SCR active species.[3] To date, there does not seem to be convincing evidence, either experimentally or theoretically, that explains why Cu/SSZ-13 has to be different from other Cu-zeolites. In our most recent studies on SCR kinetics, we discovered that, at low Cu loadings where Cu-dimer species are not spectroscopically detected, our kinetic data indicate that transient dimers can indeed form and act as reaction centers under typical low temperature NH_3−SCR reaction conditions.[9]

As part of our continuing research efforts aimed at understanding detailed SCR mechanisms and metal/zeolite structure−function relationships from both experimental and theoretical approaches, in the present study, we investigate NO chemisorption on Cu/SSZ-13 using both FTIR spectroscopy and DFT calculations. These recent studies have provided new insights into the nature of isolated Cu ion species as functions of the Si/Al ratio, Cu loading, and the presence or absence of ligands attaching to the catalytically active centers.

2. METHODS

2.1. Computational Details. DFT calculations were performed with the Vienna Ab-initio Simulation Package (VASP) code.[26,27] The projector augmented-wave (PAW)[28,29] method and the generalized-gradient approximation (GGA), using the PW91 functional,[30] were employed for the treatment of the electron−ion interactions and the exchange−correlation effects, respectively. With its PAW potentials, VASP combines the accuracy of all-electron methods with the computational efficiency of plane-wave approaches. The total energy convergence threshold was set to 10^{-8} eV, and the geometries were considered to be fully relaxed when the forces were less than 0.01 eV/Å. A 400 eV plane-wave cutoff and a single Γ-point sampling of the Brillouin zone were used for these calculations. In order to obtain an accurate density of states (DOS) for Cu, higher Monkhorst−Pack k-point grids of (5 × 5 × 5) were used. The default values of RWIGS for the PW91 pseudopotential were employed in our DOS calculations. The numbers of valence electrons are 4, 6, 3, and 11 for Si, O, Al and Cu atoms, respectively.

As is well-known, the SSZ-13 zeolite belongs to the CHA zeolite family, with a structure that is composed of 4-membered rings (4MR), 6-membered rings (6MR), and 8-membered rings (8MR), as displayed in Figure 1a. There are two equivalent ways to construct the CHA unit cell. One is the hexagonal cell with 36 symmetry-equivalent tetrahedral (T) sites and 72 O atoms. The other is a rhombohedral cell containing 12 T sites and 24 O atoms. All T sites are crystallographically equivalent and there are four nonequivalent O sites, which can be distinguished according to their participation in the different ring structures of the framework. As shown in Figure 1a, the oxygen O1 belongs to two 4MRs and one 8MR (abbreviated as (4, 4, 8)); O2 belongs to (4, 6, 8); O3 belongs to (4, 4, 6); and finally O4 belongs to (4, 8, 8). The rhombohedral unit cell was used in all of our calculations, as shown in Figure 1.

dx.doi.org/10.1021/cs500563s | ACS Catal. 2014, 4, 4093−4105

In a rhombohedral unit cell, electron deficits are generated upon replacement of Si atoms by Al atoms. Extra framework Cu ions are then required to compensate such electron deficits. For a one-electron deficit, a Cu^+ ion is required. In this case, the resulting zeolite configuration is denoted as ZCu. A two-electron deficit is compensated by a Cu^{2+} ion, and this configuration is labeled as Z_2Cu. Alternatively, a two-electron deficit can be compensated for with a Brønsted acid site (H^+) and a Cu^+ ion. The resulting configuration is labeled as HZ_2Cu. After full relaxation of the rhombohedral unit cell, the calculated equilibrium volumes of ZCu, Z_2Cu, and HZ_2Cu are the same at 823.6 $Å^3$. Detailed calculations and plots of energy as a function of volume can be found in the Supporting Information (Figure S1). As will be shown below, besides "naked" Cu ions, Cu ions with ligands (e.g., $[Cu(OH)]^+$ species) as charge balancing moieties are also considered in this study.

For the molecular adsorption calculations, the unit cells with chemisorbed NO were fully relaxed to get their equilibrium volumes, which are 823.6, 828.8, and 834.1 $Å^3$, respectively, for ZCu, Z_2Cu, and HZ_2Cu. The energy plots as a function of volume for the NO-adsorbed systems are shown in Figure S1 of the Supporting Information. The adsorption of NO has no effect on the equilibrium volume of ZCu, but it causes a slight increase of the equilibrium volumes for Z_2Cu and HZ_2Cu. We note, under the experimental conditions used here, that not all Cu sites will be occupied by NO molecules, and additionally, not every unit cell will contain a Cu atom. Because of this, there will be local strain on the unit cell which, due to its complexity, cannot be addressed in our calculations. In studying other adsorbates, unit cell lattice constants identified for the NO-adsorbed systems were used. Adsorption energies E_{ads} are calculated by the following equation:

$$E_{ads} = E_{tot} - E_{zeolite} - E_M \quad (1)$$

where E_{tot}, $E_{zeolite}$, and E_M are the total energies of the zeolite system in the presence of molecular species, the clean zeolite system, and the isolated molecules in the gas phase, respectively.

2.2. Experimental Section. Three SSZ-13 zeolite substrates with Si/Al ratios of 6, 12, and 35 were used in this study. The sample with Si/Al = 6 was synthesized in-house following the procedure described by Fickel and Lobo.[5] The high Si/Al samples (12 and 35) were also synthesized in-house, using procedures described by Deka et al.[7] Cu/SSZ-13 catalysts with various Cu/Al ratios were then prepared using traditional solution ion-exchange methods that have also been described previously.[31] Prior to ion exchange with a $CuSO_4$ solution, the as-synthesized Na/SSZ-13 samples were first exchanged to NH_4/SSZ-13. Si, Al and Cu contents were determined by elemental analysis (ICP), while the crystallinity of the zeolites was confirmed by XRD.

In situ static transmission IR experiments were conducted in a home-built cell (described in detail previously[32]) housed in the sample compartment of a Bruker Vertex 80 spectrometer. In short, powder samples were pressed onto a tungsten mesh that can be resistively heated (by passing current through the metal grid) or cooled with liquid nitrogen. Unless otherwise specified, samples were annealed in vacuum (~1×10^{-7} Torr) at 500 °C for 2 h and cooled back to ambient temperature prior to background spectra acquisition. Then NO was introduced into the cell in a pulse mode fashion (~0.005 Torr for the first pulse, until total pressure in the IR cell reached ~0.5 Torr). After equilibrium NO pressure was reached after each pulse of NO, an IR spectrum was acquired. Note that our highest NO pressure of ~0.5 Torr was specifically chosen in order to avoid formation of Cu−dinitrosyl or even polynitrosyl complexes.

3. RESULTS

3.1. DFT Results. In the SSZ-13 zeolite, previous experimental results have shown that the most favorable location for the Cu ion is in the face of a 6MR site.[5−7] Cu ions in this site have also been suggested to be catalytically active for the NH_3−SCR reaction.[5,7,12] We first examined the local structures of Cu ions in the 6MR site of ZCu and Z_2Cu, as shown in Figure 2. It was found that the Cu ions are 3-fold and

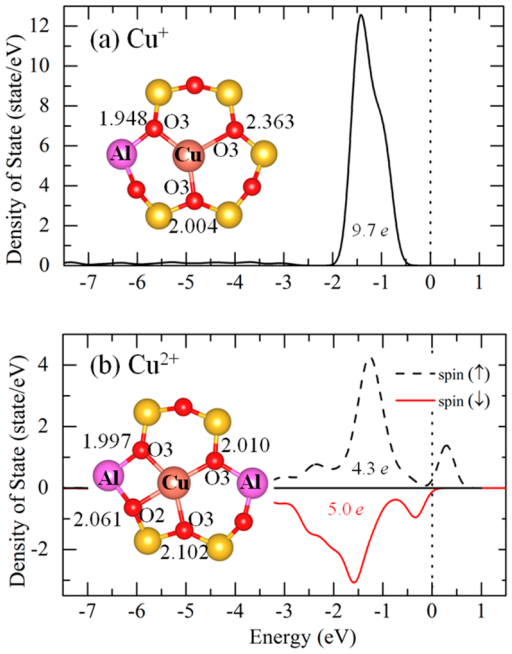

Figure 2. PDOS of Cu 3d states in (a) ZCu and (b) Z_2Cu. Insets are the local structures of Cu in the 6MR sites. Cu−O bond lengths are indicated in units of Å. Different types of lattice O atoms can be found in Figure 1. The numbers of integrated electrons from PDOS plots are shown. In (b), the dash and solid lines show spin-up- and spin-down states for Cu 3d, respectively, and the dotted vertical line highlights the location of the Fermi level. Spheres for Si and O depicted as in Figure 1, with Cu being shown as large pink balls and Al as purple ones.

4-fold coordinated to lattice O atoms for ZCu and Z_2Cu, respectively. For ZCu, the Cu ion coordinates with three O3 atoms and the shortest bond length of 1.948 Å occurs between Cu and the O3 atom adjacent to the Al-substituted site. For Z_2Cu, in addition to three O3 atoms, the Cu ion also coordinates with an O2 atom adjacent to the Al-substituted site. These results are consistent with previous computational results reported by McEwen et al.[12] Examination of the partial density of state (PDOS) for Cu ions in ZCu and Z_2Cu confirms that Cu ions are in +1 and +2 oxidation states, respectively. For ZCu, the +1 oxidation state is evidenced by the completely filled 3d state (9.7 e), as shown in Figure 2a. For Z_2Cu, a peak exists above the Fermi level in the PDOS plot of the Cu 3d spin up state indicating an electron loss in the Cu 3d state. This is confirmed by the integrated Cu 3d electrons of 4.3 e (spin up) and 5.0 e (spin down), as displayed in Figure 2b. These results demonstrate that the Cu ion has a +2 oxidation state in Z_2Cu.

dx.doi.org/10.1021/cs500563s | ACS Catal. 2014, 4, 4093−4105

Figure 3 displays the local structures of NO adsorbed on ZCu and Z_2Cu (ZCu-NO and Z_2Cu-NO), as well as the

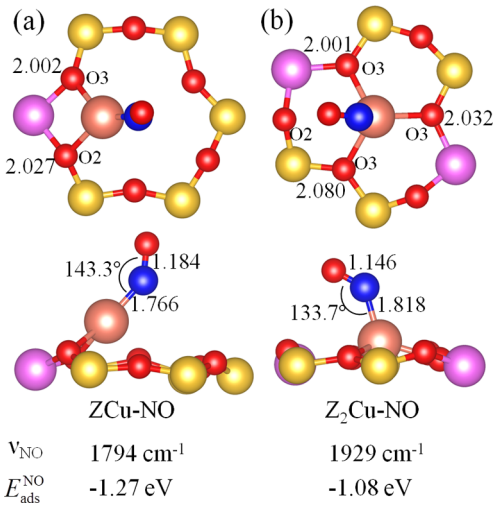

Figure 3. Top and side views of structures for NO adsorbed on ZCu and Z_2Cu, shown as (a) ZCu-NO and (b) Z_2Cu-NO, respectively. The adsorption energies calculated by eq 1 as well as NO frequencies (ν_{NO}) are presented at the bottom of the figure. The spheres for Si, O, Cu, Al atoms are same as in previous figures. The blue sphere denotes a N atom.

frequencies and the adsorption energies of NO. With NO adsorption, the Cu ions still maintain 3-fold and 4-fold coordination numbers for ZCu and Z_2Cu. For ZCu-NO, the formation of a Cu−N bond is accompanied by the breaking of two Cu−O3 bonds and the formation of a Cu−O2 bond. For Z_2Cu-NO, in contrast, the Cu−N bond formation causes cleavage of the Cu−O2 bond. The adsorption energy for NO in ZCu-NO (−1.27 eV) is 0.19 eV stronger than that in Z_2Cu-NO (−1.08 eV). This difference is consistent with the calculated Cu−N bond lengths, 1.766 Å in ZCu-NO and 1.818 Å in Z_2Cu-NO, also displayed in Figure 3. As demonstrated above, the Cu ions in ZCu and Z_2Cu are Cu^+ and Cu^{2+}, respectively. The NO adsorption energy and Cu−N bond length differences are expected to be caused by these Cu ion oxidation state differences. Note also that the interaction between the NO π^* state and the Cu 3d state forbids a linear geometry,[21] thus resulting in Cu−N−O angles of 143.3° and 133.7° for ZCu-NO and Z_2Cu-NO, respectively.

The calculated stretching vibrational frequencies (ν_{NO}) for ZCu-NO and Z_2Cu-NO are 1794 and 1929 cm^{-1}, which are consistent with computational results by using cluster[17] and periodic[21] models. Note that gas phase NO has ν_{NO} of 1896 cm^{-1}. These vibrational frequencies agree well with the calculated N−O bond lengths. The N−O bond lengths for ZCu-NO, gas phase NO and Z_2Cu-NO are 1.184, 1.169, and 1.146 Å, respectively.

NO chemisorption shown above only considers the simplest situation (i.e., naked Cu ions located in faces of 6MR). However, the practical NH_3−SCR reaction conditions are rather complicated. In order for our calculations to be more relevant, complexities are added in the following calculations. Namely, we attempt to investigate NO adsorption under three conditions: (1) on Cu sites in different charge balancing locations of the chabazite structure; (2) in the presence of Brønsted acid sites; and (3) in the presence of extra framework ligands (i.e., −OH and H_2O).

In addition to the 6MR site shown in Figure 3, SSZ-13 offers various potential sites for Cu ions. A variation of the distribution of the Al atoms among the T-sites leads to different cation structures for Cu/SSZ-13. For the location of the Cu^+ cation, our recent results show that the 6MR site is more favorable than the 8MR sites with an energy difference about 0.5 eV.[33] Göltl et al. considered eight possible different cation structures for Cu^{2+}/SSZ-13 and concluded that the most favorable structure is when both Al atoms and the Cu^{2+} cation are located within the same 6MR, with the two Al atoms distributed in a AlSiSiAl configuration.[24] By studying the CO frequencies adsorbed on the Cu^{2+} cation in different structures, they found that the change in the local environment changes the frequencies of the adsorbed CO molecule.[24] The question here is what happens to the NO molecule for such local environment changes. We systematically investigated the effect of the Cu position and Al atoms distribution on the frequencies of the adsorbed NO molecule. A detailed description can be found in the Figure S2 of the Supporting Information. It is found that the change of the Cu^+ location does not change the NO stretch frequency considerably for the ZCu-NO systems. However, for NO adsorbed on a Cu^{2+} ion, the NO frequency is dependent on not only the Cu location but also on the distribution of the two Al atoms. For example, when a Cu^{2+} ion is in a 6MR site, a change from an AlSiAl distribution to an AlSiSiAl configuration results in an increase of the NO frequency from 1901 to 1929 cm^{-1}. With the same AlSiSiAl distribution, the NO frequency varies from 1929 cm^{-1} to 1918 and 1932 cm^{-1} when the Cu position changes from the 6MR to the 8MR sites, although Cu in an 8MR is less favorable than in a 6MR site. We conclude that the local Cu^{2+} environment changes the frequencies of the adsorbed NO, which is similar to the results for CO as reported by Göltl et al.[24]

Concerning the presence of Brønsted acid sites, as shown in Figure 1, there are four nonequivalent O sites in the SSZ-13 framework. First, we investigate the simple situation where only the Brønsted acid sites exist in SSZ-13 (H/SSZ-13) (i.e., replacing one Si atom by one Al atom and using an H atom to compensate the charge deficit). These have already been investigated by DFT methods in the literature.[19,34] The stability of the Brønsted acid sites is found to decrease in the sequence of O1 > O2 > O3 > O4, which is consistent with previous results reported by Suzuki et al.[34] and Göltl et al.[19] In addition, the calculated Al−O bond length is also in line with those works. Detailed information can be found in Table S1 of the Supporting Information. Similarly, due to the existence of four nonequivalent O sites, four possible Brønsted acid site locations can be arranged next to an Al T site in Z_2Cu, namely, O1, O2, O3 and O4 sites, as shown in Figure 4. The calculated bond lengths and energies are summarized in Table 1. The introduction of a Brønsted acid site into Z_2Cu decreases the Cu coordination number from 4 to 3. The Al−O bond lengths change slightly with different locations of the Brønsted acid site. Note especially the configuration where the Brønsted acid site is located in the O3 site. In this configuration, the bond length for Cu−O3 is 2.023 Å, larger than the Cu−O3 bond lengths when Brønsted acid sites are located on O1, O2, and O4, as shown in Figure 4. It is also found that the O3 Brønsted acid site is energetically the least favorable one, with ΔE_1 = 0.88 eV, as shown in Table 1. Although the ΔE_1 values for the O2 and O4 Brønsted acid sites are rather small, the O1 Brønsted acid

dx.doi.org/10.1021/cs500563s | ACS Catal. 2014, 4, 4093−4105

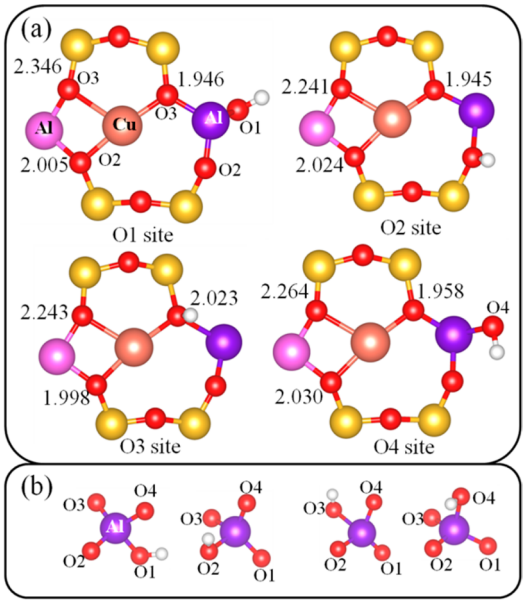

Figure 4. (a) Local structures of a six-membered ring in the presence of a Brønsted acid site and a Cu atom. (b) Corresponding local structure of the tetrahedral Al site that is adjacent to the Brønsted acid site. The spheres for Si, O, Cu, and Al atoms are the same as in previous figures. The dark Al represents the location of the tetrahedral Brønsted acid site. The small white spheres represent the H atoms.

Table 1. Al−O Bond Lengths (Å) for the Four Configurations Shown in Panel b of Figure 4[a]

Brønsted acid site	Al−O1	Al−O2	Al−O3	Al−O4	O−H	ΔE_1 (eV)
O1	**1.915**	1.696	1.800	1.693	0.977	0.00
O2	1.704	**1.881**	1.802	1.700	0.978	0.08
O3	1.700	1.696	**2.188**	1.691	0.988	0.88
O4	1.712	1.720	1.797	**1.881**	0.983	0.14

[a] ΔE_1 is the energy difference of HZ_2Cu with different locations of the Brønsted acid site, with respect to the total energy of the O1 Brønsted acid site. Positive values designate less favorable sites than the O1 Brønsted acid site.

site configuration is clearly the most stable one, and only this structure will be further considered in the following. We also note that in all configurations, the Al−O(H) bond length is always longer than the other three Al−O bonds (highlighted in Table 1).

Next, we investigate different Cu positions in HZ_2Cu by fixing the Brønsted acid site in the O1 location. Figure 5 displays the local structures of HZ_2Cu with Cu in both 6MR and 8MR positions. Cu in the 6MR site has a 3-fold coordination to lattice O atoms (two O3 and one O2); for the two positions of Cu in the 8MR sites, Cu atoms are either bonded with the O1 and O4 atoms (denoted as the 8MR_O14 site) or the O2 and O4 atoms (8MR_O24 site). All calculated Cu−O bond lengths for the three configurations are displayed in Figure 5.

Table 2 presents calculated energy differences (ΔE_2) for the three "naked" HZ_2Cu configurations, as well as configurations

Table 2. Energy Differences ΔE_2 As Defined in the Text[a]

ΔE_2 (eV)	6MR	8MR_O14	8MR_O24
HZ_2Cu	0.00	1.00	0.89
HZ_2Cu-NO	0.00	−0.07	0.08
HZ_2Cu-OH	0.00	−0.56	0.02
HZ_2Cu-H_2O	0.00	−0.18	−0.19
HZ_2Cu-(NO + OH)	0.00	−0.60	0.25

[a] The positive and negative values present less and more favorable positions, respectively, as compared to the corresponding scenario with Cu in a 6MR position.

with chemisorbed species (NO, OH, H_2O, and NO + OH), using the corresponding configurations for Cu in the 6MR site as the zero energy references. Without adsorbates, the 6MR is clearly the energetically more favorable site; the 8MR_O14 and 8MR_O24 sites are 1.00 and 0.89 eV, respectively, energetically less favorable. However, with NO and H_2O as adsorbates, the difference greatly diminishes and the 8MR sites can even become slightly more favorable (except for 8MR_O24-NO). More importantly, in the cases of OH and NO + OH as adsorbates, the 8MR_O14 conformation is energetically substantially more favorable ($\Delta E_2 \sim -0.6$ eV). In the following, more details are given on these calculated results.

As displayed in Figure 6, in all three HZ_2Cu-NO configurations, Cu displays 2-fold coordination with lattice oxygen. The adsorption of NO on HZ_2Cu in a 6MR (E_{ads}^{NO} = −0.96 eV) is weaker than that on ZCu (E_{ads}^{NO} = −1.27 eV, Figure 3). However, when NO is adsorbed on HZ_2Cu associated with

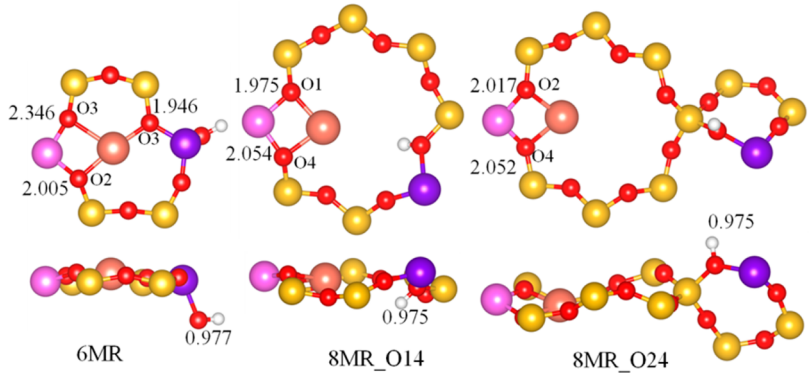

Figure 5. Local structures of three possible Cu positions (6MR, 8MR_O14 and 8MR_O24) in HZ_2Cu. Note that Al and H atoms are in the same position when varying positions of Cu and that an extended part of the zeolite is shown for Cu in the 8MR_O24, so as to show the location of both Al sites. The Brønsted acid site locates in the O1 site. The Cu−O distances (Å) are indicated in each panel. The color schemes for different atoms are the same as in previous figures, and the nonequivalent O atoms are identified in Figure 1.

dx.doi.org/10.1021/cs500563s | ACS Catal. 2014, 4, 4093−4105

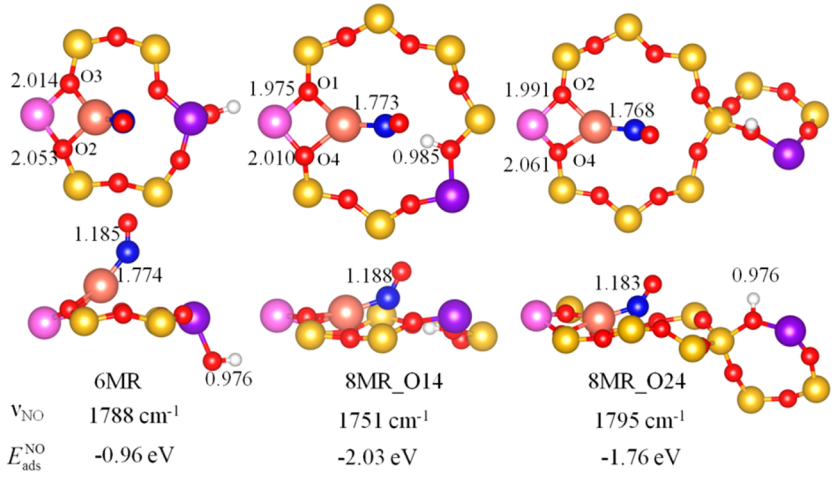

Figure 6. Local structures of NO adsorbed in a HZ_2Cu conformation with Cu in a 6MR, 8MR_O14, and a 8MR_O24 conformation. The color coding for the spheres have the same meaning as previous figures, and the given distances are bond lengths in Å units. The NO frequencies and adsorption energies of NO are indicated at the bottom of the figure.

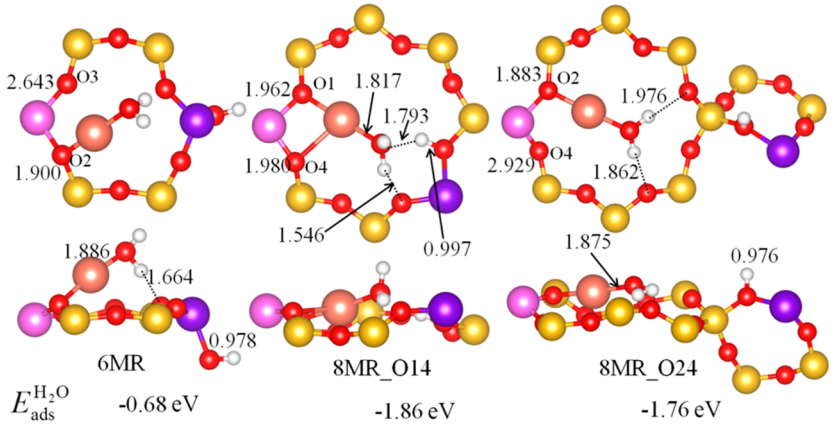

Figure 7. Local structures of H_2O adsorbed onto HZ_2Cu with Cu in the 6MR, 8MR_O14, and 8MR_O24 sites. The color coding for the spheres and given distances have the same meaning as previous figures. The adsorption energies of H_2O are indicated at the bottom of the figure.

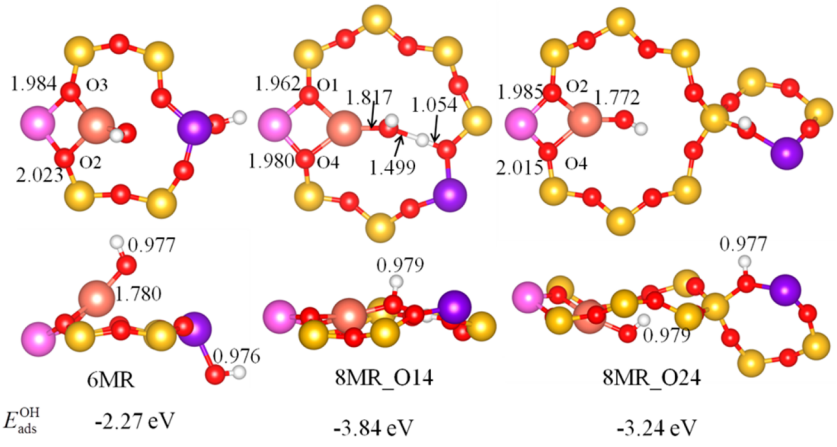

Figure 8. Local structures of OH adsorbed on HZ_2Cu with Cu in the 6MR, 8MR_O14, and 8MR_O24 sites. The color coding for the spheres and given distances have the same meaning as previous figures. The adsorption energies of OH are indicated at the bottom of the figure.

8MRs, much stronger adsorption energies are obtained. Importantly, these energies are sufficiently high to compensate for the instability of "naked" Cu ions in 8MRs, making the 8MR_O14-NO conformation the energetically more favorable configuration (Table 2). The frequencies of NO adsorbed on Cu in 6MR, 8MR_O14 and 8MR_O24 sites of HZ_2Cu are 1788, 1751, and 1795 cm^{-1}, respectively. Different from the case of Cu^+ in the ZCu-NO system, where the location of the Cu^+ results in a very weak effect on NO frequency, the NO frequency in the HZ_2Cu-NO decreases from 1788 to 1751 cm^{-1} when Cu migrates from the 6MR to the 8MR_O14 site and increases from 1788 to 1795 cm^{-1} when Cu migrates from

dx.doi.org/10.1021/cs500563s | ACS Catal. 2014, 4, 4093−4105

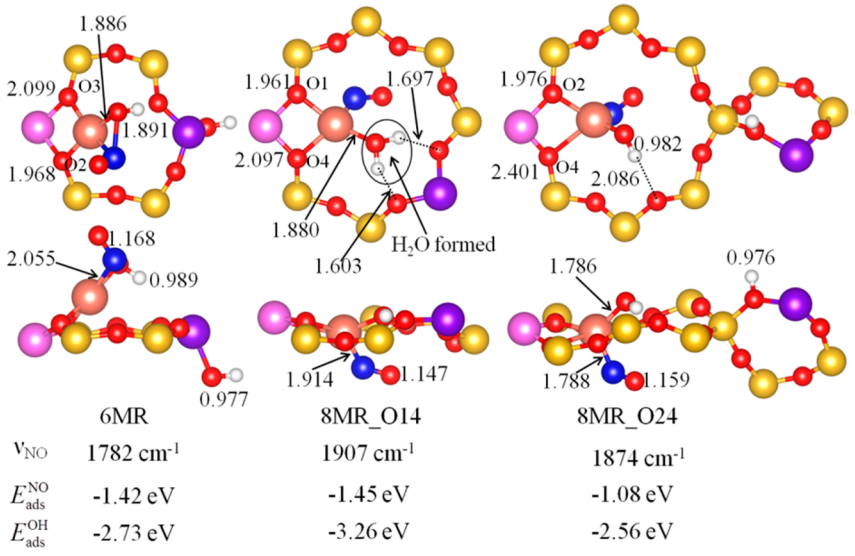

Figure 9. Local structures of NO and OH coadsorbed on HZ_2Cu with Cu in the 6MR, 8MR_O14, and 8MR_O24 sites. The color coding for the spheres and given distances have the same meaning as previous figures. The adsorption energies of NO and OH are indicated at the bottom of the figure.

the 6MR to the 8MR_O24 site. We conclude that the local environment of Cu changes the strength of the adsorbed NO molecule in the presence of a Brønsted acid site. As mentioned before, the oxidation state of Cu in HZ_2Cu should be +1 to maintain charge neutrality. These vibrational frequencies confirm that Cu in all three HZ_2Cu configurations is indeed Cu^+.

Figure 7 presents calculated results for H_2O adsorption on the three HZ_2Cu structures. Upon bond formation with H_2O, Cu only displays single coordination with lattice oxygen in 6MR and 8MR_O24, while in the 8MR_O14, 2-fold coordination with lattice oxygen still maintains. Chemisorbed H_2O has apparent hydrogen bond interactions with lattice oxygen in all cases, where the shortest distances between a H atom in H_2O and the lattice O atoms are 1.664, 1.546, and 1.862 Å in the 6MR, 8MR_O14, and 8MR_O24 sites, respectively. Again, adsorption energies for HZ_2Cu-H_2O within the 8MR_O14 and 8MR_O24 sites are substantially greater than that in 6MR, enough to overcome the instability of "naked" Cu ions in 8MRs. As such, both 8MR sites are energetically more favorable (Table 2).

The interaction between OH and HZ_2Cu is very strong, with adsorption energies in the 6MR, the 8MR_O14 and the 8MR_O24 sites being −2.36, −3.84, and −3.25 eV, respectively. As shown in Figure 8, for the most stable HZ_2Cu-OH structure in the 8MR_O14 position, the distance between the O atom of the adsorbed OH and the H atom of the Brønsted acid site is 1.499 Å. This distance is slightly longer than a valence bond which involves H but shorter than typical distances for hydrogen bonded interactions. This quasi bond formation extensively stabilizes the chemisorbed hydroxyl, giving a ΔE_2 value of −0.56 eV as shown in Table 2. In addition, this quasi bond formation elongates the O−H bond length of the Brønsted acid site (1.054 Å), as compared to the Brønsted acid site without OH adsorption (0.975 Å). It is reported that GGA and hybrid functionals lead to very different results for the location of the cation d and s states relative to the energy bands of the framework.[20] In order to compare results obtained with a hybrid functional to the GGA-PW91 functional used in this study, we recalculated the HZ_2Cu-OH systems using the hybrid HSE06 functional.[35] By using the HSE06 functional, the calculated values of the total energy differences (ΔE_2) are found to be −0.59 and 0.07 eV for Cu in a 8MR_O14 and a 8MR_O24 sites, respectively. There is no difference between these results and those calculated by the GGA-PW91 functional which are −0.56 and 0.02 eV for Cu in 8MR_O14 and 8MR_O24 sites, respectively (shown in Table 2). We therefore conclude that the HSE06 hybrid functional does not change the OH stabilization effect of Cu in the 8MR and the energetic order. However, it has been reported that large discrepancies arise when using the two functional to calculate adsorption energies.[21] By using the HSE06 functional, the calculated adsorption energies of OH on Cu in a HZ_2Cu conformation are −1.88, −3.31, and −2.52 eV for Cu in the 6MR, 8MR_O14, and 8MR_O24, respectively. These values are considerably lower than the corresponding values calculated by using the GGA-PW91 functional, with differences at 0.49, 0.52, and 0.73 eV, respectively. A detailed comparison between our results calculated with HSE06 functional and results found in the literature is shown in Section 4 of the Supporting Information.

Finally, calculated results on HZ_2Cu-$(NO + OH)_{ads}$ are shown in Figure 9. In our calculations, NO and OH are restricted to the same side of 6MR while they are placed on two sides of 8MR to release space crowding. Interestingly, in the case for Cu in the 6MR site, NO and OH interact to form HONO upon relaxation, an important intermediate proposed previously in NH_3−SCR.[36] In the 8MR sites, they remain separated upon relaxation. For Cu in the 6MR site, coadsorption with OH does not significantly change the NO vibrational frequency (1782 cm^{-1}), as compared to that of NO adsorption alone (1788 cm^{-1}, Figure 6). When NO and OH are coadsorbed on Cu in the 8MR_O14 site, the relaxed structure shows H_2O formation between the adsorbed OH and the proton from the Brønsted acid site. The O−H bond lengths in the formed H_2O are 1.014 and 1.025 Å. In 8MR_O14 and the 8MR_O24 sites, NO vibrational frequencies are 1907 and 1874 cm^{-1}, respectively, confirming that in both cases, Cu ions

dx.doi.org/10.1021/cs500563s | ACS Catal. 2014, 4, 4093−4105

are in +2 oxidation states. Finally, for Cu in the 8MR_O14 and the 8MR_O24 sites, coadsorption weakens the interactions between Cu and the adsorbates. For example, for Cu in the 8MR_O14 site, the adsorption energies of NO and OH are −1.45 and −3.26 eV upon coadsorption. However, when these species are adsorbed separately, the adsorption energies are −2.03 (Figure 6) and −3.84 eV (Figure 8), respectively.

3.2. FTIR Results. Previous studies have shown that in Cu-ion-exchanged zeolites, locations of Cu ions are influenced by multiple factors including zeolite type, Si/Al ratio, Cu ion exchange level (i.e., Cu loading), and sometimes, synthesis methods.[4] For the simple SSZ-13 structure, Cu ion locations can be readily varied by changing Si/Al ratios and Cu ion exchange levels. In this study, we synthesized three SSZ-13 samples with different Si/Al ratios. Table 3 presents the Si and Al contents for these samples, and the corresponding Si/Al ratios (6, 12 and 35) calculated on the basis of these values. Note that during the subsequent ion exchange step to obtain Cu/SSZ-13 samples, no Si or Al leaching was found, and therefore, these Si/Al ratios were maintained.

Table 3. Si, Al Contents and the Corresponding Si/Al Ratios of the Three SSZ-13 Samples Studied Here

SSZ-13 sample	Si content (wt %)	Al content (wt %)	Si/Al
1	30.4	5.03	6
2	40.3	3.23	12
3	43.4	1.20	35

As has been addressed in detail in the previous section, a naked Cu^{2+} ion balances two negative framework charges (as Z_2Cu), a naked Cu^+ ion balances one negative framework charge (as ZCu), and a Cu^+/H^+ pair balances two negative framework charges (as HZ_2Cu). It is also shown in the section above that an −OH group binds strongly with a naked Cu^+ ion. In this case, Cu^+ is oxidized to Cu^{2+}, although the nominal charge for this copper center is still +1, that is, $[Cu^{II}(OH)]^+$. Obviously, this species also only balances one negative framework charge. For the formation of stable Z_2Cu, two framework Al sites, placed in close proximity, are required. Previous studies have shown that the number of accessible Al T sites around a given Al T site approximately follows a Poisson distribution.[37,38] This means that the probability of stable Z_2Cu formation decreases exponentially as Si/Al ratios rise. Very recently, Verma et al. calculated the maximum Z_2Cu formation in a 6MR as a function of Si/Al ratios. Indeed, the expected exponential decrease as a function of Si/Al ratio was found.[23] Clearly, at very high Si/Al ratios (e.g., 35), Z_2Cu formation becomes highly unlikely. Yet, under humid and ambient conditions, experimental studies show that Cu ions remain in the +2 oxidation state irrespective of Si/Al ratio; thus, for Cu/SSZ-13 samples with low Si/Al and high Cu/Al ratios, as well as samples with high Si/Al ratios, some Cu^{2+} ions are likely present as $[Cu^{II}(OH)]^+$. In our most recent publication, the detection of an OH vibrational band at 3650 cm^{-1} (absent for SSZ-13 in H- and Na-forms) is direct evidence for the existence of $[Cu^{II}(OH)]^+$.[10] In a recent publication by Lezcano-Gonzalez et al.,[25] a 3655 cm^{-1} band, which becomes more intense as Cu loading increases, was assigned to the same $[Cu^{II}(OH)]^+$ species, and these authors calculated the ν_{OH} in $[Cu^{II}(OH)]^+$ to be 3660 cm^{-1}.[25] Similarly, Giordanino et al. also assigned a stretching OH band at 3657 cm^{-1} to ν_{OH} in $[Cu^{II}(OH)]^+$.[39]

Figure 10 presents IR spectra obtained after NO exposure of a Cu/SSZ-13 sample (Si/Al = 6, Cu/Al = 0.45) annealed in vacuum at 500 °C prior to NO adsorption. Note that these spectra have been published elsewhere;[32] however, they are replotted here because they are key to understanding NO chemisorption on the other samples shown below. IR bands centered at ∼1808, 1900, and 2165 cm^{-1} appear immediately after the introduction of the first small NO aliquot (0.017 Torr). With the introduction of additional NO doses, the intensities of all of these bands increased together with slight changes in frequencies, and new features developed as well. Notably, new bands at ∼1785, 1910, 1930 (weak), 1948, and 2249 (weak) cm^{-1} appeared at higher NO pressures. While more details will be given below, briefly, bands at 1785 and 1808 cm^{-1} are attributed to NO adsorbed on Cu^+ sites; bands within the range of ∼1850−1950 cm^{-1} are assigned to NO adsorbed on Cu^{2+} sites; the broad band centered at ∼2165 cm^{-1} is attributed to NO^+ species, and finally, the weak 2249 cm^{-1} feature belongs to adsorbed N_2O. The stabilities of the adsorbed species represented by these IR absorption features are very different. Bands centered at 1948 and 1930 cm^{-1} disappear completely after a brief (∼10 min) evacuation at 300 K. The intensity of the 1808 cm^{-1} band (NO on Cu^+) decreases dramatically in the first 10 min of evacuation, but it retains a small fraction of its intensity. Bands in the 1880−1920 cm^{-1} spectral region, although with diminished intensities, are also still present after this evacuation step. The most resistant IR feature to evacuation is the one centered at around 2165 cm^{-1}.

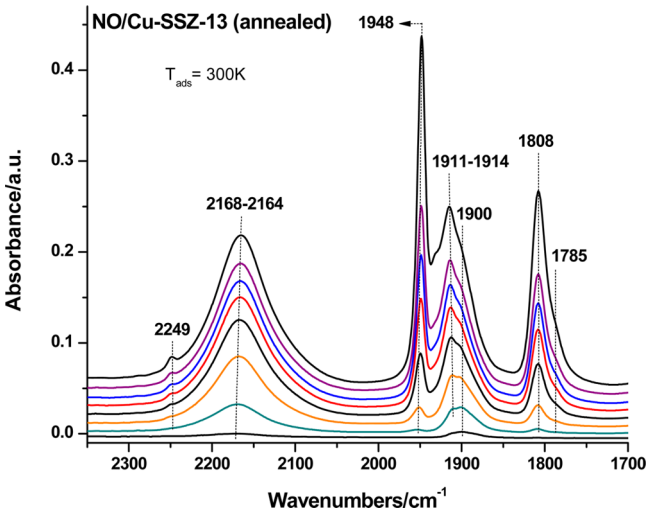

Figure 10. Series of selected IR spectra obtained after exposure of a Cu/SSZ-13 sample (Si/Al = 6, Cu/Al = 0.4) to NO 300 K. The sample was annealed in vacuum at 773 K for 2 h prior to IR measurements.

Figure 11a presents ambient temperature IR spectra of adsorbed NO collected on a Cu/SSZ-13 sample (Si/Al = 6, Cu/Al = 0.03) annealed in vacuum at 500 °C prior to NO adsorption. Note that the Cu loading in this sample is substantially lower than the one used to collect data for Figure 10. However, the sequence for band development as a function of NO pressure and the relative signal intensities among various bands are strikingly similar to that shown in Figure 10. Still, some subtle differences are evident. Notably, after the first NO dose, a rather distinctive Cu^{2+}−NO band was found at 1883

dx.doi.org/10.1021/cs500563s | ACS Catal. 2014, 4, 4093−4105

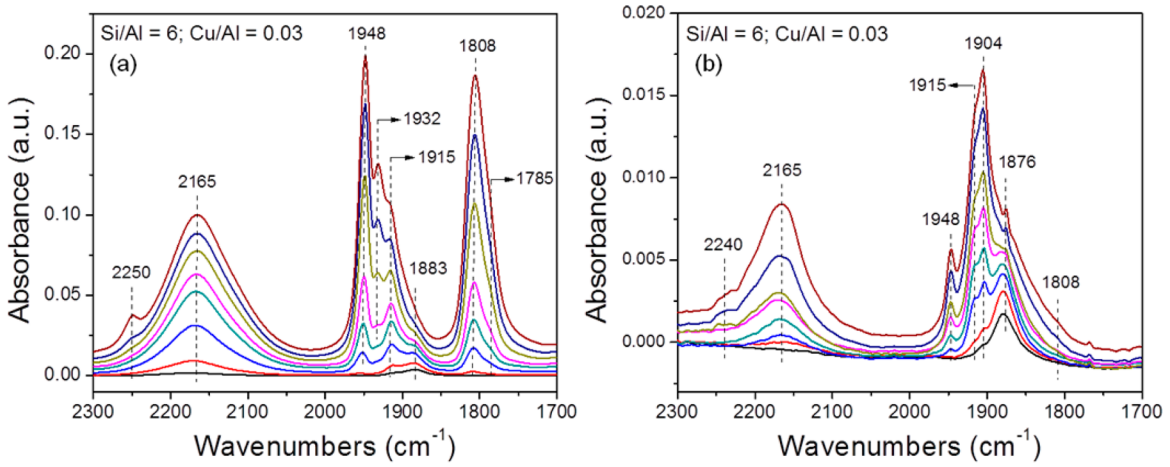

Figure 11. (a) Series of selected IR spectra obtained after exposure of a Cu/SSZ-13 sample (Si/Al = 6, Cu/Al = 0.03) to NO 300 K. The sample was annealed in vacuum at 773 K for 2 h prior to IR measurements. (b) Series of selected IR spectra obtained after exposure of a Cu/SSZ-13 sample (Si/Al = 6, Cu/Al = 0.03) to NO 300 K. The sample was annealed in vacuum at 423 K for 2 h prior to IR measurements. Note that after this latter low-temperature annealing treatment, the sample is only partially dehydrated.

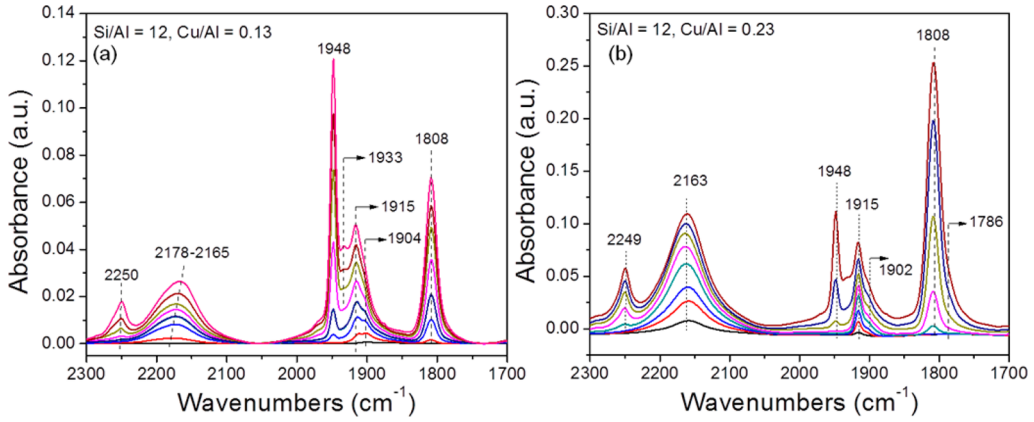

Figure 12. (a) Series of selected IR spectra obtained after exposure of a Cu/SSZ-13 sample (Si/Al = 12, Cu/Al = 0.13) to NO 300 K. The sample was annealed in vacuum at 773 K for 2 h prior to IR measurements. (b) Series of selected IR spectra obtained after exposure of a Cu/SSZ-13 sample (Si/Al = 12, Cu/Al = 0.23) to NO 300 K. The sample was annealed in vacuum at 773 K for 2 h prior to IR measurements.

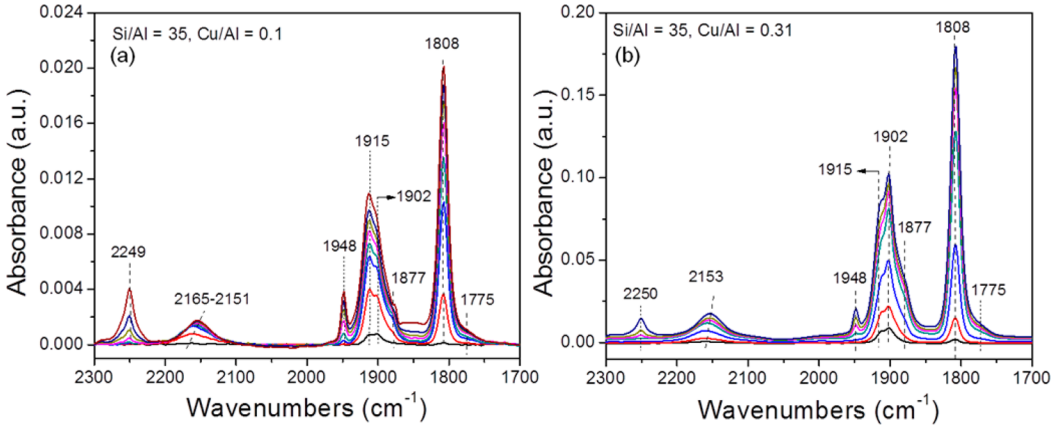

Figure 13. (a) Series of selected IR spectra obtained after exposure of a Cu/SSZ-13 sample (Si/Al = 35, Cu/Al = 0.10) to NO 300 K. The sample was annealed in vacuum at 773 K for 2 h prior to IR measurements. (b) Series of selected IR spectra obtained after exposure of a Cu/SSZ-13 sample (Si/Al = 35, Cu/Al = 0.31) to NO 300 K. The sample was annealed in vacuum at 773 K for 2 h prior to IR measurements.

cm^{-1}, slightly red-shifted as compared with the higher Cu loading sample. Also, the ~1930 cm^{-1} feature appears to be much better resolved on this low-Cu loaded sample at high NO pressures. Figure 11b presents ambient temperature NO IR spectra collected on the same sample but only annealed in vacuum to 150 °C prior to NO adsorption. Note that following such a treatment, the sample is still partially hydrated.[10] Interestingly, IR spectra are markedly different in this case, and

dx.doi.org/10.1021/cs500563s | ACS Catal. 2014, 4, 4093−4105

key observations are the following: (1) the 1808 cm^{-1} is very weak, suggesting Cu^{2+} autoreduction to Cu^{+} essentially does not occur; (2) the 1883 cm^{-1} band red-shifts slightly to 1876 cm^{-1} at low NO pressures while, with increasing NO pressure, a new and strong Cu^{2+}−NO band develops at 1904 cm^{-1}; and (3) the relative intensity for the 1948 cm^{-1} feature, as compared to other Cu^{2+}−NO bands at lower frequencies, is much weaker. Meanwhile, the ∼1930 cm^{-1} band cannot be resolved.

Figure 12 presents ambient temperature NO IR spectra collected on Cu/SSZ-13 samples (Si/Al = 12, Cu/Al = 0.13 (a) and Cu/Al = 0.23 (b)) annealed in vacuum at 500 °C prior to NO adsorption. For both samples, Cu^{2+}−NO bands at ∼1902 and 1915 cm^{-1} develop first, and with increasing NO pressure, a strong band at 1948 cm^{-1} grows. The ∼1930 cm^{-1} feature only becomes reasonably well-defined at the highest NO pressures. Note that the relative signal intensities change as a function of Cu/Al ratios. Specifically, the Cu^{+}−NO band at 1808 cm^{-1} becomes much stronger than Cu^{2+}−NO bands at Cu/Al = 0.23, suggesting that the extent of autoreduction is enhanced as Cu loading increases. It is also clear that the relative signal intensity for N_2O (at ∼2250 cm^{-1}) is higher for the Si/Al = 12 samples as compared to the Si/Al = 6 ones shown in Figures 10 and 11.

Finally, Figure 13 depicts NO adsorption IR spectra acquired on Cu/SSZ-13 samples (Si/Al = 35, Cu/Al = 0.1 (a) and Cu/Al = 0.31 (b)) annealed in vacuum at 500 °C prior to NO adsorption at ambient temperature. For both samples, vibrational bands at ∼2165, 1915, 1902, and 1808 cm^{-1} appear immediately after the first NO dose. With increasing NO pressure, an N_2O band at ∼2250 cm^{-1}, Cu^{2+}−NO bands at 1948 and 1877 cm^{-1}, and a Cu^{+}−NO band at 1775 cm^{-1} start to develop. Three key findings are worth pointing out for these two samples: (1) markedly different from samples with lower Si/Al ratios, the 1948 cm^{-1} feature appears to be much weaker as compared to other Cu^{2+}−NO bands (between 1880 and 1915 cm^{-1}); (2) the Cu^{+}−NO band at 1808 cm^{-1} is very strong, indicating facile Cu^{2+} autoreduction to Cu^{+} for these samples; and (3) the intensity for the N_2O band at ∼2250 cm^{-1} becomes comparable to the NO^{+} feature at ∼2160 cm^{-1} for these two samples. In contrast, for lower Si/Al samples, the intensity for the N_2O band is generally somewhat to considerably weaker than NO^{+}.

4. DISCUSSION

One of the key attributes of Cu/SSZ-13 is its structural simplicity; the CHA structure is constructed by stacking double 6MRs so that all tetrahedral sites (T-sites, Al and Si) are in equivalent structural positions. Cu ions have been initially suggested to be present only as isolated monomers (Cu^{2+} and Cu^{+}), and that they solely occupy one extra-frame site, that is, faces of 6MRs.[5] In view of this evident structural simplicity, we[3] and others[4,5] have suggested that Cu/SSZ-13 offers an excellent opportunity to elucidate some long-standing questions regarding NH_3−SCR, including the nature of the catalytically active centers and detailed reaction mechanism(s). With continuing research efforts, however, it has become evident that the situation is significantly more complicated than initially thought. First, it is an oversimplification to suggest one type and one location for the catalytic centers within Cu/SSZ-13.[8,13,31] In line with studies on other Cu/zeolite SCR catalysts, the nature and location of Cu species are influenced by multiple factors including structure of the zeolites, Si/Al ratios, Cu loadings, and synthesis methods.[4,36,40] Second, oxidation states, locations, and chemical nature of the Cu catalytic centers are expected to vary as a function of reaction conditions; therefore, only in operando spectroscopic techniques applicable to NH_3−SCR are, in principle, able to accurately monitor these dynamic variations allowing the establishment of accurate structure−function relationships. Although great progress has been reported in studies of these materials under in operando conditions,[9,10] using probe molecules to identify the location and characterize the nature of catalytically relevant Cu species is clearly an important component to achieve this goal.

In our previous study,[32] using ^{14}NO and ^{15}NO as probe molecules, on samples with vacuum annealing, oxidization and reduction treatments, as well as with and without the presence of moisture, we were able to gain detailed information on the nature of various isolated ionic Cu species. For example, we divided Cu^{2+}−NO bands into two groups based on their relative stabilities in our previous study, and denoted the less stable Cu^{2+}−NO species (giving rise to the 1948 and 1932 cm^{-1} bands) to $Cu^{2+}\cdots NO(II)$ and the more stable Cu^{2+}−NO species (giving rise to bands from 1870 to 1915 cm^{-1}) to $Cu^{2+}\cdots NO(I)$. We also realized that in the presence of moisture, $Cu^{2+}\cdots NO(II)$ partially converts to $Cu^{2+}\cdots NO(I)$. However, we were unable to give more detailed assignments in our previous study. In the present work, with experimental aid from samples with various Si/Al and Cu/Al ratios (Figures 11−13) and new information from DFT calculations, detailed assignments of most of the FTIR spectral features are achieved, as will be discussed below.

Cu^{2+}−NO species that gives rise to the 1948 cm^{-1} band are discussed first. Note that this band is very sharp (fwhm <10 cm^{-1}), suggesting that (1) relevant Cu^{2+} ions occupy a highly specified charge balancing site and that (2) no other chemisorbed species are in close vicinity to perturb NO vibrations. It is also clear that, on samples with lower Si/Al ratios (6 and 12, Figures 10−12), this band is the dominant Cu^{2+}−NO species at high NO pressures, while for the sample with a Si/Al ratio of 35, the relative intensity of this band diminishes dramatically (Figure 13). From the DFT results shown in Figure 3, good agreement is found for the Z_2Cu-NO species with our experimental results. Therefore, it is quite certain that the 1948 cm^{-1} band is due to NO adsorbed on Cu^{2+} sites in the faces of the 6MR. The 1932 cm^{-1} band is also likely NO adsorbed on Cu^{2+} sites in the faces of 6MR, but with an energetically less favorable structure (see Figure S2 in Supporting Information); that is, two Al T sites are separated by one Si T site instead of two, as shown in Figure 3b.

Next, Cu^{2+}−NO species giving rise to bands from 1870 to 1915 cm^{-1} are discussed. Note first that these bands develop prior to the 1948/1932 cm^{-1} bands during NO adsorption and maintain longer during evacuation. Note also that we discovered previously that the relative intensities of these bands are enhanced in the presence of moisture at the expense of the 1948/1932 cm^{-1} features. In the present study, on the partially dehydrated Si/Al = 6 sample (Figure 11b), these bands also dominate over the 1948/1932 cm^{-1} features. For the Si/Al = 35 samples, these bands still dominate even when the samples have been fully dehydrated (annealed in vacuum at 500 °C). These experimental findings strongly suggest the following: (1) stronger binding between Cu^{2+} and NO for the NO species that give rise to bands from 1870 to 1915 cm^{-1}; (2) these bands are likely associated with H_2O and/or −OH ligands. While binding with a H_2O molecule does not change the oxidation state of a

dx.doi.org/10.1021/cs500563s | ACS Catal. 2014, 4, 4093−4105

copper ion, binding with an −OH ligand converts Cu^+ to Cu^{2+}. Interestingly, a H_2O ligand effectively moderates the energy difference between Cu^+ ions in the faces of 6MR and 8MR; an −OH ligand even makes 8MR sites energetically much more favorable (Table 2). The calculated NO vibrational frequencies shown in Figure 9, therefore, strongly suggest that the experimental bands from 1870 to 1915 cm^{-1} can be assigned to $[Cu^{II}(OH)]^+$-NO species located close to 8MR. The reason why two or three bands overlap in this region can be argued to be caused by the slight differences of local environments in the vicinity of the Cu ion centers. We note that in previous studies,[7] Cu^{2+} ions have been suggested to only occupy faces of 6MR and they even stay in such positions under SCR reaction conditions. From both DFT calculations and simple chemisorption FTIR experiments, we show in this study that the previous understandings on Cu^{2+} ion location may need to be revised.

The nature of the Cu^+−NO species is discussed in this section. As has been well-known, Cu^+ formation is due to the so-called "autoreduction" which occurs when Cu-ion-exchanged zeolite materials are annealed in vacuum. Therefore, Cu^+ formation in this highly idealized condition may not correlate with Cu^+ formation under standard NH_3−SCR reaction conditions found by others. For example, the sample used to collect spectra shown in Figure 10 has much higher Cu content than the sample used to collect data for Figure 11a, yet under the highly idealized NO chemisorption conditions, the resulting spectra are quite similar. Nevertheless, by comparing the 1808 cm^{-1} bands obtained from samples with various Si/Al ratios (Figures 10−13), some interesting and subtle differences are noticed: (1) For the Si/Al = 6 samples, the shoulder band at ∼1786 cm^{-1} is better resolved than for samples with higher Si/Al ratios. (2) The full width at half-maximums (fwhms) of the 1808 cm^{-1} band for samples with different Si/Al ratios are very different. At high NO pressures, the fwhms are ∼32, ∼22, and ∼15 cm^{-1}, for samples with Si/Al ratios of 6, 12 and 35, respectively. This finding indicates that the 1808 cm^{-1} band should not be assigned to a single Cu^+−NO species. From Figures 3 and 6, the calculated structures giving rise to the 1794, 1788, and 1795 cm^{-1} bands can all contribute to the experimental 1808 cm^{-1} band. By changing the Cu^+ locations, there is a 7 cm^{-1} shift for the NO frequency in the Cu^+-NO conformation, which is consistent with that reported in the literature.[21] Note specifically, with the decrease in Si/Al ratios (i.e., the increase in Brønsted acid site density), contribution of the 1808 cm^{-1} band from HZ_2Cu is expected to increase. This seems to nicely explain the fwhm increase with decreasing Si/Al ratios. For both Cu^{2+}−NO and Cu^+−NO species, there appears to be a systematic 10−20 cm^{-1} difference between the experimental NO vibrations and their DFT counterparts (the calculated values are smaller). In this sense, we do not have a good assignment for the experimental shoulder band at ∼1786 cm^{-1}.

Finally, the experimental NO^+ bands (at ∼2160 cm^{-1}) and the N_2O species (at ∼2250 cm^{-1}) are briefly discussed. There have been some historic debates on the nature of the NO vibrational band at ∼2130−2170 cm^{-1}. Work done by Hadjiivanov et. al[41] appeared to settle the argument, and this band on a bare zeolite is now generally agreed to be a NO^+ species adsorbed on extra framework cationic sites. In a recent publication, we assigned this band on Cu/SSZ-13 to a NO^+ species as well.[13] Moreover, our in situ solid state NMR results strongly suggest that this band directly associates with Cu ions. Accordingly, we assigned this NO species to a Cu^+−NO^+ complex formed by charge transfer from NO to Cu^{2+}. In the present study, from the comparison between Figure 10 and Figure 11a, although the sample used to collect spectra for Figure 10 has a Cu loading more than 10 times higher than that used to collect spectra for Figure 11a, the relative NO^+ band signal intensities (as compared to the Cu^{2+}−NO and Cu^+−NO bands) are quite similar. Moreover, from Figures 11−13, as the Si/Al ratios increase (i.e., Brønsted acid site density decreases), the general trend is that the relative NO^+ band signal intensities decrease. This is especially obvious for the Si/Al = 35 samples. Therefore, the NO^+ species do not appear to adsorb directly on Cu ion sites, but rather, they occupy cationic positions that compensate framework negative charges. However, they must be in close proximity to the Cu ions in order to allow for the interactions observed with our prior in situ NMR experiments.[13] Although DFT calculations in either case could not match the experimental NO vibrational frequencies for this species, the effect of partial charge on the frequency of NO in the gas phase was studied to support this assignment. As shown in Figure S3 of the Supporting Information, the frequency of NO increases as the charge on NO increases from negative to positive values. Similar predictions on the CO vibrational frequencies were reported to follow the trend CuCO < $(CuCO)^+$ < $(CuCO)^{2+}$ by using a cluster model.[15] Positive charge of NO means loss of electron density from NO. In this sense, the ∼2160 cm^{-1} bands is produced by electron transfer from NO to a site in Cu/SSZ-13 where NO adsorbed. Thus, the assignment of NO^+ at ∼2160 cm^{-1} bands is reasonable, although the corresponding conformation associated with this NO^+ species remains unclear.

Finally we comment on the N_2O band centered at ∼2250 cm^{-1}. As shown in Figures 10−13, this band's position is independent of the samples, which have different ratios of Si/Al and Cu/Al. This result is supported by the DFT calculations. As shown in Figure S4 in Supporting Information, the frequencies of N−O in N_2O adsorbed on ZCu, Z_2Cu, and HZ_2Cu, which are 2367, 2339, and 2362 cm^{-1}, have only slight variations. These results are also quite similar to a cluster model estimate of 2360 cm^{-1}.[17] It is concluded that the frequency of N−O in N_2O is largely independent of the chemical environment of Cu in Cu/SSZ-13. Under NH_3−SCR reaction conditions, N_2O is typically undetectable on freshly prepared Cu-SSZ-13 catalysts at relatively low Cu loadings. Over high Cu loading fresh catalysts, it does form (although yields are typically very low) from NH_4NO_3 decomposition. On hydrothermally aged catalysts, N_2O formation is greatly enhanced above ∼400 °C; its formation in this case is believed to be catalyzed by CuO_x clusters formed during catalyst aging. In the present study, N_2O formation may originate from NO disproportionation or NO reduction by Cu ions. Again, under such highly idealized experimental conditions, one cannot correlate N_2O formation here with that observed during NH_3−SCR reactions.

5. CONCLUSIONS

By varying Si/Al and Cu/Al ratios, Cu/SSZ-13 samples with different Cu ion extra-framework locations are obtained. For samples fully dehydrated in high vacuum, three chemisorbed NO species coexist upon NO adsorption. These are NO^+ species (∼2170−2160 cm^{-1}), Cu^{2+}−NO species (1950−1850 cm^{-1}), and Cu^+−NO species (1808−1770 cm^{-1}). The relative signal intensities for these bands vary significantly with

dx.doi.org/10.1021/cs500563s | ACS Catal. 2014, 4, 4093−4105

changing Si/Al ratios. With the aid of DFT calculations, the species responsible for these vibrations can be assigned in detail. Table 4 summarizes the assignments by comparing experimental and computational results. DFT results show that Cu ions are 3-fold and 4-fold coordinated to lattice O atoms and present in +1 and +2 oxidation states for ZCu and Z_2Cu, respectively. In addition, the calculated stretching vibrational frequencies for Cu^{2+}−NO and Cu^{+}−NO are 1929 and 1794 cm^{-1}, respectively. Furthermore, Cu^{+} ions are shown to be substantially stabilized by −OH ligands (as $[Cu^{II}(OH)]^{+}$), making extra-framework sites in 8MR energetically more favorable than 6MR sites (the energetically more favorable sites for "naked" Cu^{2+} ions). FTIR results coupled with DFT calculations allow us to conclude that NO molecules do bind stronger on $[Cu^{II}(OH)]^{+}$ located in 8MR than naked Cu^{2+} ions in the 6MR. This new knowledge that Cu^{2+} ions are indeed stabilized with ligands in 8MR sites should greatly aid our understanding in Cu/CHA SCR catalysts.

Table 4. Main Findings from the Experimental and Theoretical Results of NO Frequencies (cm^{-1}) in Different Configurations

NO frequency (cm^{-1})	experimental results	computational results
Cu^{2+}−NO	1850−1950	1895−1932
$[Cu(II)OH]^{+}$−NO	1870−1915	1874, 1907
Cu^{+}−NO	1770−1808	1794, 1788, 1795
Cu−N_2O	∼2250	2367, 2339, 2362
Cu^{+}−NO^{+}	2160−2170	-

■ ASSOCIATED CONTENT

Supporting Information

Plots of energy as a function of volume, local structures, energy differences and bond lengths, locations of the Brønsted acid site, comparisons between HSE06 and PW91 functionals, total and adsorption energies, charge effect on the frequency of NO in gas phase. This material is available free of charge via the Internet at http://pubs.acs.org.

■ AUTHOR INFORMATION

Corresponding Authors

*E-mail: js.mcewen@wsu.edu.

*E-mail: chuck.peden@pnnl.gov.

Notes

The authors declare no competing financial interest.

■ ACKNOWLEDGMENTS

For the authors from Washington State University, this work was supported by institutional funds provided to J.-S.M. from the Voiland School of Chemical Engineering and Bioengineering. This work was partially funded by USDA/NIFA through Hatch Project #WNP00807 titled: "Fundamental and Applied Chemical and Biological Catalysts to Minimize Climate Change, Create a Sustainable Energy Future, and Provide a Safer Food Supply". For those of us from Pacific Northwest National Laboratory (PNNL), financial support was provided by the U.S. Department of Energy (DOE), Office of Energy Efficiency and Renewable Energy, Vehicle Technologies Program. A portion of the research (including both computer time for DFT and experimental FTIR work) was performed using EMSL, a national scientific user facility sponsored by the Department of Energy's Office of Biological and Environmental Research and located at PNNL. PNNL is a multiprogram national laboratory operated for the U.S. DOE by Battelle. We also thank Ms. Kathy Helling for her useful comments on the manuscript.

■ REFERENCES

(1) Bull, I.; Xue, W. M.; Burk, P.; Boorse, R. S.; Jaglowski, W. M.; Koermer, G. S.; Moini, A.; Patchett, J. A.; Dettling, J. C.; Caudle, M. T. *Copper CHA zeolite catalysts*. Patent no. US7601662 B2, 2009.

(2) Andersen, J.; Bailie, J. E.; Casci, J. L.; Chen, H.-Y.; Fedeyko, J. M.; Foo, R. K. S.; Rajaram, R. R. *Transition metal/zeolite SCR catalysts*. Patent no. WO/2008/132452, 2008.

(3) Gao, F.; Kwak, J.; Szanyi, J.; Peden, C. F. *Top. Catal.* **2013**, *56*, 1441−1459.

(4) Deka, U.; Lezcano-Gonzalez, I.; Weckhuysen, B. M.; Beale, A. M. *ACS Catal.* **2013**, *3*, 413−427.

(5) Fickel, D. W.; Lobo, R. F. *J. Phys. Chem. C* **2010**, *114*, 1633−1640.

(6) Korhonen, S. T.; Fickel, D. W.; Lobo, R. F.; Weckhuysen, B. M.; Beale, A. M. *Chem. Commun.* **2011**, *47*, 800−802.

(7) Deka, U.; Juhin, A.; Eilertsen, E. A.; Emerich, H.; Green, M. A.; Korhonen, S. T.; Weckhuysen, B. M.; Beale, A. M. *J. Phys. Chem. C* **2012**, *116*, 4809−4818.

(8) Hun Kwak, J.; Zhu, H.; Lee, J. H.; Peden, C. H. F.; Szanyi, J. *Chem. Commun.* **2012**, *48*, 4758−4760.

(9) Gao, F.; Walter, E. D.; Kollar, M.; Wang, Y.; Szanyi, J.; Peden, C. H. F. *J. Catal.* **2014**, *319*, 1−14.

(10) Kwak, J. H.; Varga, T.; Peden, C. H. F.; Gao, F.; Hanson, J. C.; Szanyi, J. *J. Catal.* **2014**, *314*, 83−93.

(11) Kispersky, V. F.; Kropf, A. J.; Ribeiro, F. H.; Miller, J. T. *Phys. Chem. Chem. Phys.* **2012**, *14*, 2229−2238.

(12) McEwen, J. S.; Anggara, T.; Schneider, W. F.; Kispersky, V. F.; Miller, J. T.; Delgass, W. N.; Ribeiro, F. H. *Catal. Today* **2012**, *184*, 129−144.

(13) Kwak, J. H.; Lee, J. H.; Burton, S. D.; Lipton, A. S.; Peden, C. H. F.; Szanyi, J. *Angew. Chem., Int. Ed.* **2013**, *52*, 9985−9989.

(14) Yang, X.; Wu, Z.; Moses-Debusk, M.; Mullins, D. R.; Mahurin, S. M.; Geiger, R. A.; Kidder, M.; Narula, C. K. *J. Phys. Chem. C* **2012**, *116*, 23322−23331.

(15) Schneider, W. F.; Hass, K. C.; Ramprasad, R.; Adams, J. B. *J. Phys. Chem.* **1996**, *100*, 6032−6046.

(16) Schneider, W. F.; Hass, K. C.; Ramprasad, R.; Adams, J. B. *J. Phys. Chem. B* **1997**, *101*, 4353−4357.

(17) Schneider, W. F.; Hass, K. C.; Ramprasad, R.; Adams, J. B. *J. Phys. Chem. B* **1998**, *102*, 3692−3705.

(18) C. Hass, K.; F. Schneider, W. *Phys. Chem. Chem. Phys.* **1999**, *1*, 639−648.

(19) Göltl, F.; Hafner, J. *J. Chem. Phys.* **2012**, *136*, 064501.

(20) Göltl, F.; Hafner, J. *J. Chem. Phys.* **2012**, *136*, 064502.

(21) Göltl, F.; Hafner, J. *J. Chem. Phys.* **2012**, *136*, 064503.

(22) Bates, S. A.; Verma, A. A.; Paolucci, C.; Parekh, A. A.; Anggara, T.; Yezerets, A.; Schneider, W. F.; Miller, J. T.; Delgass, W. N.; Ribeiro, F. H. *J. Catal.* **2014**, *312*, 87−97.

(23) Verma, A. A.; Bates, S. A.; Anggara, T.; Paolucci, C.; Parekh, A. A.; Kamasamudram, K.; Yezerets, A.; Miller, J. T.; Delgass, W. N.; Schneider, W. F.; Ribeiro, F. H. *J. Catal.* **2014**, *312*, 179−190.

(24) Göltl, F.; Bulo, R. E.; Hafner, J.; Sautet, P. *J. Phys. Chem. Lett.* **2013**, *4*, 2244−2249.

(25) Lezcano-Gonzalez, I.; Deka, U.; Arstad, B.; Van Yperen-De Deyne, A.; Hemelsoet, K.; Waroquier, M.; Van Speybroeck, V.; Weckhuysen, B. M.; Beale, A. M. *Phys. Chem. Chem. Phys.* **2014**, *16*, 1639−1650.

(26) Kresse, G.; Furthmüller, J. *Phys. Rev. B* **1996**, *54*, 11169.

(27) Kresse, G.; Hafner, J. *Phys. Rev. B* **1993**, *47*, 558.

(28) Blöchl, P. E. *Phys. Rev. B* **1994**, *50*, 17953.

(29) Kresse, G.; Joubert, D. *Phys. Rev. B* **1999**, *59*, 1758−1775.

(30) Perdew, J. P.; Wang, Y. *Phys. Rev. B* **1992**, *45*, 13244.

(31) Gao, F.; Walter, E. D.; Karp, E. M.; Luo, J.; Tonkyn, R. G.; Kwak, J. H.; Szanyi, J.; Peden, C. H. F. *J. Catal.* **2013**, *300*, 20−29.
(32) Szanyi, J.; Kwak, J. H.; Zhu, H.; Peden, C. H. F. *Phys. Chem. Chem. Phys.* **2013**, *15*, 2368−2380.
(33) Zhang, R.; McEwen, J.-S. Thermodynamic stability and ab initio X-ray absorption modeling of Cu-SSZ-13: Influence of reactants, intermediates, and products in the SCR of NO_x. **2014**, in preparation.
(34) Suzuki, K.; Sastre, G.; Katada, N.; Niwa, M. *Phys. Chem. Chem. Phys.* **2007**, *9*, 5980−5987.
(35) Krukau, A. V.; Vydrov, O. A.; Izmaylov, A. F.; Scuseria, G. E. *J. Chem. Phys.* **2006**, *125*, 224106.
(36) Brandenberger, S.; Kröcher, O.; Tissler, A.; Althoff, R. *Catal. Rev.* **2008**, *50*, 492−531.
(37) Rice, M. J.; Chakraborty, A. K.; Bell, A. T. *J. Catal.* **1999**, *186*, 222−227.
(38) Goodman, B. R.; Hass, K. C.; Schneider, W. F.; Adams, J. B. *Catal. Lett.* **2000**, *68*, 85−93.
(39) Giordanino, F.; Vennestrom, P. N. R.; Lundegaard, L. F.; Stappen, F. N.; Mossin, S.; Beato, P.; Bordiga, S.; Lamberti, C. *Dalton Trans.* **2013**, *42*, 12741−12761.
(40) Centi, G.; Perathoner, S. *Appl. Catal., A* **1995**, *132*, 179−259.
(41) Hadjiivanov, K.; Saussey, J.; Freysz, J. L.; Lavalley, J. C. *Catal. Lett.* **1998**, *52*, 103−108.